

Observation of particle hole asymmetry and phonon excitations in non-Fermi liquid systems: A high-resolution photoemission study of ruthenates

KALOBARAN MAITI,^(*) RAVI SHANKAR SINGH, AND V.R.R. MEDICHERLA

Department of Condensed Matter Physics and Materials Science, Tata Institute of Fundamental Research, Homi Bhabha Road, Colaba, Mumbai - 400005, INDIA

PACS. 71.10.Hf – Non Fermi liquid ground states, electron phase diagrams and phase transitions in model systems.

PACS. 63.20.Kr – Phonon - electron and phonon - phonon interactions.

PACS. 71.45.Gm – Exchange, correlation, dielectric and magnetic response functions, plasmons.

Abstract. –

We investigate the temperature evolution of the electronic states in the vicinity of the Fermi level of a non-Fermi liquid (NFL) system, CaRuO₃ using ultra high-resolution photoemission spectroscopy; isostructural SrRuO₃ exhibiting Fermi liquid behavior despite similar electron interaction parameters as that of CaRuO₃, is used as a reference. High-energy resolution in this study helps to reveal particle-hole asymmetry in the excitation spectra of CaRuO₃ in contrast to that in SrRuO₃. In addition, we observe signature of phonon excitations in the photoemission spectra of CaRuO₃ at finite temperatures while these are weak in SrRuO₃.

Recent observations of various bulk properties in normal phase of high temperature superconductors [1], *d* and *f* electrons at quantum critical points [2], low dimensional systems [3] *etc.*, exhibit deviations from Fermi-liquid (FL) behavior, the most fundamental paradigm in solid-state physics [4]. Such non-Fermi liquid (NFL) behavior has often been attributed to strong electron correlations and/or charge fractionalizations [5]. Interestingly, CaRuO₃, a 3-dimensional orthorhombically distorted perovskite exhibits NFL behavior at low temperatures, while isostructural SrRuO₃ exhibits Fermi liquid (FL) behavior [6]. Magnetic measurements reveal ferromagnetic ground state in SrRuO₃ (Curie temperature, $T_C \sim 165$ K). However, CaRuO₃ does not exhibit long range order.

The average Ru-O-Ru bond angle is slightly different in these two compounds (150° in CaRuO₃ and 165° in SrRuO₃). It was believed that the decrease in the electron hopping interaction strength, t , due to smaller Ru-O-Ru angle in CaRuO₃ leads to an increase in effective electron correlation strength, U/W (U = electron-electron Coulomb repulsion strength, $t \propto W \sim$ bandwidth), and hence the NFL behavior appears in CaRuO₃ [6]. However, a recent study based on band structure calculation and photoemission spectroscopy [7] shows that the width of various *d*-bands remains almost the same across the series and U/W is essentially

^(*) Corresponding author: kbmaiti@tifr.res.in

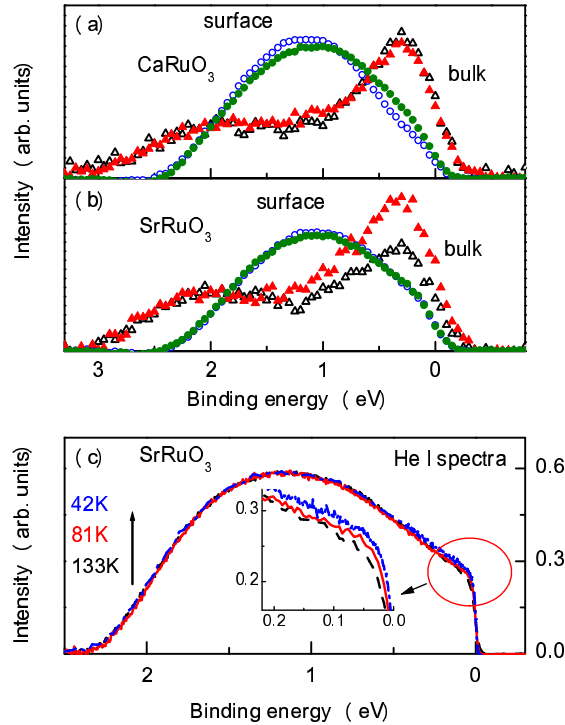


Fig. 1 – (color online) Surface (circles) and bulk (triangles) spectral functions of (a) CaRuO₃ and (b) SrRuO₃. Closed symbols represent spectra at 300 K and the open ones represent spectra at 48 K and 35 K for CaRuO₃ and SrRuO₃, respectively. (c) High resolution He I spectra of SrRuO₃. The dashed, solid and dot-dashed lines represent the spectrum at 133 K, 81 K and 42 K, respectively. The inset shows the expanded view of the same spectra near ϵ_F .

identical in both the compounds. Thus, significantly different ground state properties despite similar electron interaction parameters in these systems pose a challenging question and any comparative study will provide an ideal opportunity to investigate various fundamental factors responsible for NFL behavior. With this motivation, we report our results on the evolution of the electronic structure of CaRuO₃ and SrRuO₃ as a function of temperature employing photoemission spectroscopy with ultra high resolutions (1.4 meV for ultraviolet photoemission spectroscopy and 300 meV for *x*-ray photoemission spectroscopy). Significantly different temperature evolutions of the bulk spectra of SrRuO₃ and CaRuO₃ reveal the signature of different magnetic ground states in their electronic structure. Very high resolution enabled us to probe the signature of particle-hole asymmetry and phonon excitations in the vicinity of the Fermi level, ϵ_F in the temperature evolution of photoemission spectra in CaRuO₃ in contrast to that in SrRuO₃.

Photoemission measurements were performed on high quality samples [7] at a base pressure of 3×10^{-11} torr using a SES2002 Gammadata Scienta analyzer and monochromatized photon sources. The details of the sample preparation and characterization has been described elsewhere [7]. The sample surface was cleaned by *in situ* scraping. The cleanliness and reproducibility of the spectra were ascertained after each cycle of scraping.

It is now realized that the surface electronic structure of transition metal oxides [7–9] is

significantly different from the bulk electronic structures due to different symmetry, surface reconstruction *etc.* that occur at the surface. Thus, we have extracted the surface and bulk spectral functions of SrRuO₃ and CaRuO₃ using high-resolution spectra at Al $K\alpha$ (1486.6 eV) and He II (40.8 eV) radiations across T_C and shown in Fig. 1. Interestingly, the sharp feature at ϵ_F in the bulk spectra, known as coherent feature representing the delocalized electronic states reduce drastically below T_C in SrRuO₃ with respect to the incoherent feature intensity around 2 eV (signature of correlation induced localized states). Such reduction in intensity is consistent with the results from band structure calculations [10, 11] and can be attributed to the finite exchange splitting leading to a shift of the minority spin contributions above ϵ_F . Thus, these results suggest that the coherent feature in the 35 K spectrum primarily appears due to up-spin contributions and that up- and down-spin Fermi surfaces are significantly different.

Within the ferromagnetic phase, the spectral functions are relatively insensitive to the change in temperature in the wide energy scale as evident in the He I (21.2 eV) spectra in Fig. 1(c). The decrease in temperature leads to a small increase in intensity near ϵ_F (signature of the resonant feature) as evident in the high-resolution spectra shown in an expanded scale in the inset. It is difficult to realize such evolutions merely from the Fermi-Dirac distribution function as the energy range of intensity enhancement is much larger (> 200 meV) than expected ($\epsilon_F \pm 2k_B T$) energy range. Various state-of-the-art calculations based on dynamical mean field theory predicted such temperature-induced changes in a correlated Fermi liquid system (see Fig. 39 and corresponding discussions in Ref. [12]). These thermal effects in the electron density fluctuations were used to demonstrate the metal-insulator transitions in a correlated electron system as a function of temperature. While such effects are often smeared out due to the disorder introducing a dip at ϵ_F , the high resolution employed in this study helped to reveal this effect in real systems. In sharp contrast, the bulk spectral functions in CaRuO₃ (see Fig. 1(a)) are essentially identical in the wide energy scale down to 48 K. High resolution spectra do not exhibit temperature evolutions as observed in SrRuO₃.

Interestingly, the surface spectra shown in Fig. 1(a) and 1(b) for both CaRuO₃ and SrRuO₃ exhibit very small intensity at ϵ_F at all the temperatures. Resolution broadening of 300 meV of the intense higher binding energy features in the surface spectra is expected to enhance the intensity at ϵ_F . Instead, observed small intensities indicate that the spectral density at ϵ_F in the surface electronic structure is negligible. Thus, the intensity at ϵ_F (coherent feature) in the He I spectra essentially correspond to the bulk electronic structure. Such a scenario has indeed been demonstrated in a similar system, SrVO₃ [13], where the dispersion and mass enhancement of the electronic states at ϵ_F in the ultra-violet spectra are identical to the bulk of the system.

In order to investigate the anomalous behavior in CaRuO₃ further, we probe the spectral evolution close to ϵ_F . The energy resolution and the Fermi level at each temperature are determined by the experiments on high purity polycrystalline Ag sample as shown in Fig. 2(a) for the spectrum at 20 K. Interestingly, the experimental spectrum (circles) is almost exactly reproduced by bare Fermi-Dirac distribution function (line) without using any broadening due to the instrumental resolution. This is again confirmed by comparing the energy derivative of both the spectral functions across ϵ_F . A broadening more than 1.5 meV (FWHM) exhibits deviations from the experimental spectrum and is consistent with the measured resolution broadening in Xe 5p levels. Since transport occurs in the low energy scale (\sim meV), *it is necessary to achieve such high resolution to critically investigate these properties.* Using this *state-of-the-art* energy resolution achieved in this instrument, we investigate the spectral changes in SrRuO₃ and CaRuO₃ as shown in Fig. 2(c) and 2(d), respectively. All the spectra, normalized at the binding energy 100 meV ($\gg k_B T$), appear to cross each other at ϵ_F as

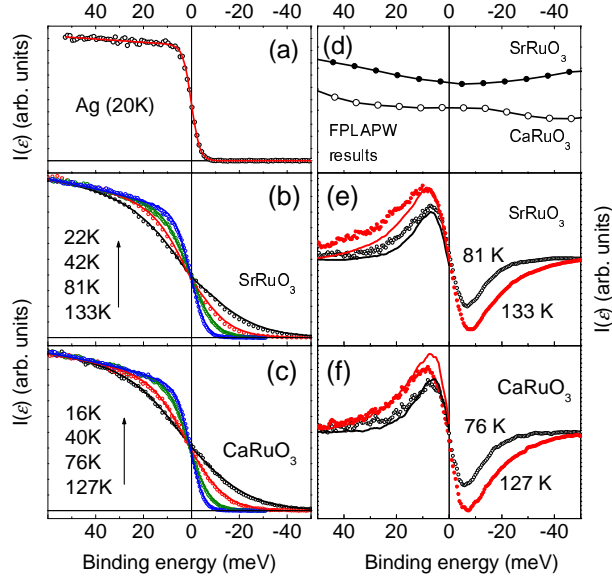


Fig. 2 – (color online) (a) Valence band spectra of Ag at 20 K near ϵ_F . The line represents the bare Fermi-Dirac distribution at 20 K. (b) and (c) show the temperature evolution of the spectral functions near ϵ_F for SrRuO₃ and CaRuO₃, respectively. (d) Total density of states of SrRuO₃ and CaRuO₃ from the Full Potential Linearized Augmented Plane Wave Calculations. (e) and (f) show the difference spectra obtained by subtracting the spectra at higher temperatures from the lowest temperature spectra of SrRuO₃ and CaRuO₃, respectively. The lines represent the same subtracted spectra above ϵ_F inverted and superimposed onto the lower energy part.

expected in a system of fermions following Fermi-Dirac distribution function.

The electrical conduction, σ , of a Fermi-liquid scales as T^{-2} and can be expressed as $\sigma = \frac{n(\epsilon)e^2\tau}{m^*}$ ($n(\epsilon)$ = carrier density in the vicinity of ϵ_F , τ = scattering rate and m^* = effective mass). Thus, in addition to the temperature dependence of τ , the shape of $n(\epsilon)$ and its evolution with temperature play a significant role in determining the temperature dependence of electronic conduction. Various recent studies [14] suggest that a simple power law dependence of $n(\epsilon)$ captures most of the physical properties associated to the electronic states close to ϵ_F . Thus, we simulate the photoemission response, $I(\epsilon) = \int d\epsilon' \times n(\epsilon') \times F(\epsilon', T) \times G(\epsilon, \epsilon', \gamma)$ considering $n(\epsilon) = n_0 + n_1 |\epsilon - \epsilon_F|^\alpha$, $F(\epsilon, T)$ is the Fermi-Dirac distribution function and G is the Gaussian broadening. We find that $\alpha = 0.5 \pm 0.05$ provides a good description of the spectra for both CaRuO₃ and SrRuO₃ for $BE > 2k_B T$ suggesting an influence of disorder in the electronic structure as also observed in other oxides [15, 16]. Interestingly, the full width at half maximum (FWHM) of the Gaussian needed to simulate the experimental spectra is significantly large compared to 1.4 meV expected from the instrument resolution function. Most notable change is observed in the case of CaRuO₃. While FWHM in SrRuO₃ is always < 8 meV, the values in CaRuO₃ are 14.5, 11.0, 7.8 and 7.5 meV at the temperatures of 127 K, 76 K, 40 K and 16 K respectively. Such significant temperature dependence of FWHM suggests influence of electron-phonon coupling in the electronic structure of CaRuO₃ [17].

In addition, the spectral weight transfer appears to be different in the two systems; e.g. the spectral weight transfer from 0-20 meV binding energy range to the energy region above ϵ_F for a change in temperature from 22 K to 42 K in SrRuO₃ is significantly larger compared

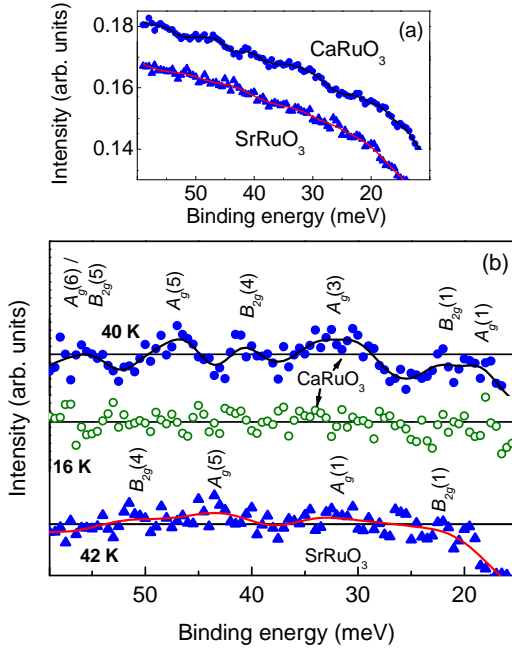


Fig. 3 – (color online) (a) The expanded raw spectra of CaRuO_3 and SrRuO_3 at 40 K in the binding energy range 20-60 meV. (b) Spectral features obtained by subtracting the simulated spectral function shown in Fig. (2) at different temperatures. $A_g(1)$ = RuO_6 z -rotation, Ca; $A_g(3)$ = RuO_6 rotation/stretching; $A_g(5)$ = Ca(y), RuO_6 stretching/bending; $A_g(6)$ = O-Ru-O bendings; $B_{2g}(1)$ = Ca(x), RuO_6 breathing; $B_{2g}(4)$ = O-O stretching; $B_{2g}(5)$ = O-Ru-O bendings as per the assignments in Refs. [22].

to that observed for similar temperature change (16 K to 40 K) in CaRuO_3 . A careful look at the spectra reveals two major differences between the two systems. Firstly, the intensities very close to ϵ_F ($|\epsilon - \epsilon_F| < k_B T$) exhibit an anomaly between the fit and experimental spectra. In order to bring out this point, we subtract the spectral functions at different temperatures from the lowest temperature spectra and show them in Fig. 2(e) and 2(f). The lines represent the spectral differences above ϵ_F , superimposed after inversion onto the difference spectra below ϵ_F . In the case of SrRuO_3 , the difference spectra are almost symmetric with respect to ϵ_F for ($|\epsilon - \epsilon_F| < k_B T$) as expected for a Fermi-liquid system. The differences observed around 10 - 50 meV binding energies may be attributed to the temperature induced gradual population of the coherent feature as shown in the inset of Fig. 1 [12]. In sharp contrast, the spectra in CaRuO_3 reveal unusual evolution with temperature; the spectral weight transferred above ϵ_F is larger than the reduction in intensity below ϵ_F . This is clearly in contrast to the expected trend based on band structure results shown in Fig. 2(d), which shows higher intensity above ϵ_F in SrRuO_3 suggesting a larger spectral weight transfer than that in CaRuO_3 . *Increase in temperature populates the hole states, which could be probed efficiently using high energy resolution.* Thus, the anomaly observed in Fig. 2(f) clearly reveals the asymmetric excitations between electrons and holes (particle-hole asymmetry) [18] in CaRuO_3 .

In addition, the spectral function of CaRuO_3 exhibits pronounced oscillations compared to that in SrRuO_3 at 40 K as shown in Fig. 3(a). This can clearly be seen in Fig. 3(b), where we show the spectral functions after subtracting the fits shown by lines in Fig. 2(c) and 2(d). The

oscillations are weak in SrRuO₃ and appear at different binding energies; the experimental data for both CaRuO₃ and SrRuO₃ were collected in the same set up with both the samples mounted together on the same sample holder. *The observation of such oscillations is unusual and has only been possible for the first time in the photoemission spectroscopy due to the very high-energy resolution employed in this study.* It is to note here that such oscillations in density of states was observed in point contact [19], tunneling studies [20], and was attributed to the electron-phonon coupling effect [21]. We, thus, compare the energy positions of the peaks with the phonon response observed in the Raman spectra in various recent studies [22]. Interestingly, all the signals observed here correspond to rotation/stretching/bending of RuO₆ octahedra, and could be assigned based on the Raman spectra and subsequent lattice dynamics calculations.

Interestingly, the distinct peaks at 40 K in CaRuO₃ spectrum become invisible at 16 K. The reduction in temperature leads to a decreased degree of electron-phonon coupling. However, the disappearance of the features at 16 K compared to the observation at 40 K may need attention. While it may be likely that the signature of coupling is below the noise level of the measurements, further studies are required (both theoretical and experimental) to probe this effect. We believe that these results would help to initiate investigations in this direction.

In SrRuO₃, the electron-phonon coupling appears to be weaker and total 4 modes corresponding to breathing modes of RuO₆ octahedra and O-Ru-O bending could be observed in the energy range studied. The spectrum in CaRuO₃, however, exhibit many additional phonon modes. It is to note here that all the additional modes in CaRuO₃ correspond to RuO₆ rotation/stretching, different O-Ru-O bending. This indicates that a smaller Ru-O-Ru angle in CaRuO₃ is more susceptible for strong scattering of electrons by the lattice. Interaction of electrons and lattice vibrations is known to be crucial to determine various exotic material properties such as colossal magnetoresistance, pseudogap phase in high-temperature superconductors [23,24]. This study indicates that the role of electron-phonon coupling in various novel material properties needs critical considerations.

NFL behavior is often found experimentally in a phase in the proximity of quantum critical point, where the NFL ground state is related to magnetic instability [2]. Evidence of the proximity of such quantum critical behavior has indeed been observed in the recent studies in high-temperature superconductors [25]. Various studies suggest that existence of low-dimensionality in these systems leads to charge fractionalization and hence NFL behavior manifests as has been shown in one-dimensional systems possessing decoupled charge and spin excitations [26,27]. The signature of particle-hole asymmetry and phonon excitations in the spectral functions of CaRuO₃ observed in this study provide evidences to consider additional parameters in the study of NFL behavior.

The authors acknowledge useful discussions with Prof. P.W. Anderson, Princeton, USA.

REFERENCES

- [1] C.G. Olson *et al.*, Phys. Rev. B **42**, 381 (1990); J. Orenstein and A.J. Millis, Science **288**, 468 (2000).
- [2] G.R. Stewart, Rev. Mod. Phys. **73**, 797 (2001).
- [3] F.D.M. Haldane, J. Phys. C: Solid State Phys. **14**, 2585 (1981).
- [4] D. Pines, P. Nozieres, The Theory of Quantum Liquids (Benjamin, New York, 1969); G. Grimvall, The Electron-Phonon Interaction in Metals (North Holland, New York, 1981).
- [5] J.D. Denlinger *et al.*, Phys. Rev. Lett. **82**, 2540 (1999); G.-H. Gweon, J.W. Allen, and J.D. Denlinger, Phys. Rev. B **68**, 195117 (2003); D. Orgad *et al.*, Phys. Rev. Lett. **86**, 4362 (2001).
- [6] L. Klein, L. Antognazza, T. H. Geballe, M. R. Beasley, and A. Kapitulnik, Phys. Rev. B **60**,

- 1448 (1999); P. Khalifah, I. Ohkubo, H. Christen, and D. Mandrus, Phys. Rev. B **70**, 134426 (2004); Y.S. Lee *et al.*, Phys. Rev. B **66**, 041104(R) (2002).
- [7] K. Maiti and R.S. Singh, Phys. Rev. B **71**, 161102(R), (2005).
- [8] K. Maiti, P. Mahadevan, and D.D. Sarma, Phys. Rev. Lett. **80**, 2885 (1998); K. Maiti and D.D. Sarma, Phys. Rev. B **61**, 2525 (2000); K. Maiti, Ashwani Kumar, D.D. Sarma, E. Weschke, and G. Kaindl, Phys. Rev. B **70**, 195112 (2004).
- [9] K. Maiti *et al.*, Europhys. Lett. **55**, 246 (2001); K. Maiti *et al.*, Phys. Rev. B **73**, 052508 (2006).
- [10] D.J. Singh, J. Appl. Phys. **79**, 4818 (1996).
- [11] K. Maiti, Phys. Rev. B **73** 235110 (2006).
- [12] A. Georges, G. Kotliar, W. Krauth, and M.J. Rozenberg, Rev. Mod. Phys. **68**, 13 (1996).
- [13] T. Yoshida *et al.*, Phys. Rev. Lett. **95**, 146404 (2005).
- [14] S. Florens, and M. Vojta, Phys. Rev. B **72**, 115117 (2005); G.-H. Gweon *et al.*, Phys. Rev. Lett. **85**, 3985 (2000).
- [15] B.L. Altschuler, and A.G. Aronov, Solid State Commun. **30**, 115 (1979).
- [16] D.D. Sarma *et al.*, Phys. Rev. Lett. **80**, 4004 (1998).
- [17] T. Valla, A. V. Fedorov, P. D. Johnson, and S. L. Hulbert, Phys. Rev. Lett. **83**, 2085 (1999).
- [18] P.W. Anderson, Nature Phys. **2**, 626 (2006).
- [19] I.K. Yanson *et al.*, Phys. Rev. B **67**, 024517 (2003).
- [20] J. Geerk *et al.*, Phys. Rev. Lett. **94**, 227005 (2005).
- [21] F. Marsiglio, M. Schossmann, and J.P. Carbotte, Phys. Rev. B **37**, 4965 (1988).
- [22] N. Kolev *et al.*, Phys. Rev. B **66**, 014101 (2002); M.N. Iliev *et al.*, Phys. Rev. B **59**, 364 (1999); D. Kirillov *et al.*, Phys. Rev. B **51**, 12825 (1995).
- [23] A.J. Millis, Nature **392**, 147 (1998).
- [24] P. Littlewood and Šimon Kos, Nature **438**, 435 (2005), N. Mannella *et al.*, Nature **438**, 474 (2005).
- [25] T. Valla *et al.*, Science **285**, 2110 (1999).
- [26] T. Valla *et al.*, Nature **417**, 627 (2002).
- [27] D. Orgad *et al.*, Phys. Rev. Lett. **86**, 4362 (2001).